2D metallic tungsten material

Bo Zhang[a], Veronika Cicmancova[b], Jhonathan Rodriguez Pereira[b], Jaroslav Kupcik[c], Petr Kutalek[e], Tomas Wagner[a, b]

[a.]Department of General and Inorganic Chemistry, Faculty of Chemical Technology, University of Pardubice, Studentska 573, 532 10 Pardubice, Czech Republic

[b.]Center of Materials and Nanotechnologies, Faculty of Chemical Technology, University of Pardubice, Nam. Cs. Legii 565, 530 02 Pardubice, Czech Republic

[c.]Institute of Inorganic Chemistry, ASCR, 250 68 Husinec-Řež Czech Republic.

[d.]Department of Physical Chemistry Faculty of Chemical Technology, University of Pardubice, Studentska 573, 532 10 Pardubice, Czech Republic

[e.]Joint Laboratory of Solid State Chemistry, University of Pardubice, Studentska 84, 532 10 Pardubice, Czech Republic

ABSTRACT

2D metallic material is an important group member in 2D material family. Many applications have been applied in the catalysis and devices. In this paper, we present a novel method to prepare the tungsten 2D material, which is simple and powerful. The W thin film is deposited via magnetron sputtering. As-deposited tungsten thin film is able to be exfoliated with wet and dry methods. We show a clear layered structure of the tungsten thin film from the cross sectional view. Via the exfoliation, an large area 2D tungsten monolayer is obtained. After oxidation, the 2D material shows potentials in electric signal transport.

KEY WORDS: *2D material, magnetron sputtering, thin film, monolayer, polycrystalline structure*

INTRODUCTION

Since the discovery of graphene exfoliation [1], the study of 2D materials attracts more attention [2] [3],[4],[5]. Meanwhile, more 2D materials are prepared, including 2D metallic materials[6], transition metal dichalcogenides [7], 2D metal oxides [8], 2D polymers [9], 2D perovskites [10], etc. Among all 2D materials, 2D metallic material is an important research field, for its various applications in catalysis, electronic devices [2]. 2D metallic material is a

family which owns many nano structures, such as nano rings [11], nano wheels[12], nano ribenons[13], nano belts [14], nano discs [15], nano plates [16], and etc. All these structures are closely linked to the synthesis methods, which can be divided according to top-down or bottom up strategies [17]. The synthesis of metallic 2D material is often processed in aqueous environment with the assistance of templates [2]. In the other words, the templates can be "hard" or "soft", which confine the growth of the materials in interlayers [18],[19]. In the other words, the principle of templates is to restrict the growth of materials in some specific directions [2]. In recent years, a method of compression synthesis has been invented, which works in a mechanical way by cycling size reduction of material. Up to now, Ag, Au, Al, Bi and Fe nanosheets have been successfully prepared via this method [20],[21],[22]. Most of the methods discussed above are related to non-layered metal or alloy. However, more complicated methods are invented to synthesis the layered metallic crystals, including molecular beam epitaxy [23], [24]. Many layered crystal structure has been successfully synthesized, for instance silicene[25], gemanene[23], antimonene [26], etc.

The dimensions are important for 2D metallic material. Larger size and smaller thickness are often preferred [17]. As discussed above, the morphology and dimension are varied in different synthetic methods [27]. The single atom thick Fe membrane shows 0.26 nm. However, the lateral dimension is only 1-2 nm [28] . Therefore, the thinner nanosheets or membranes are difficult to have a large size, because the 2D morphology is not favored from the standpoint of thermodynamics. All the nano materials have tendency to transform into isotropic shape to minimize the surface-to-volume ratio[29]. Metallic material generally has an excellent electrical transportation property. Except for application of electric transportation, the 2D metallic materials are also investigated on the field of catalysis [31], surface enhanced Raman scattering [32], sensing [33], solar cell [34], etc.

We invented a new method to synthesis 2D material. Many chalcogenide 2D materials have been successfully prepared with this method in our group [35]，[36]. In this paper, as-sputtered tungsten thin film is observed in a stack of 2D monolayers. The stack of 2D monolayers can be exfoliated via sonication in distilled water or oxidation in furnace. Further studies show a more complicated structure with tungsten thin film after exfoliation. The understanding of conductivity in exfoliated 2D tungsten monolayers can be helpful for designing new electronic devices.

MATERIALS AND METHODS

Preparation of W thin film: The W thin film is sputtered onto the Si wafer (coated with 5nm SiO_2) via RF magnetron sputtering 60W for 20 mins.

The exfoliation of W thin film: In the wet methods, The W was sonicated for 5 mins and 120 mins. After sonication, tungsten 2D layers remained on the silicon wafer. The W samples are referred as "W sample". In the dry method, the oxidation of W thin film was oxidized in an environment of 20% oxygen and 80% helium (with 400 degree Celsius) for 1 hour. The sample is referred as "WO_3 sample".

The characterizations of sample: The optical images of the tungsten thin film and monolayer are taken by the BX51. Transmission electron microscopy (TEM) measurements were performed on a JEOL JEM 3010 TEM microscope, where the W or WO_3 thin films were transferred onto a carbon-coated Cu grid. Morphology of the tungsten thin film in nano scale was investigated by a scanning electron microscope (JEOL JSM7500F) at 10kV. The chemical composition of WO_3 films was determined by X-ray photoelectron spectroscopy (XPS, ESCA 2SR, Scienta-Omicron) using monochromatic Al Kα source (1486.6 eV). The binding energy scale was referenced to adventitious carbon (284.8 eV). Depth profiling was made using a Focus FDG 150/15 ion source with Ar ion beam operated at 1keV and rastered over 3 x 3 mm^2 area. The height of tungsten monolayers are measured by AFM Solver Pro M, NT-MDT in semi-contact mode. The conductive AFM captures the information of the surface morphology and current distribution simultaneously. In the circuit, the tip is negatively charged and the tungsten thin film is positively charged at 0.12V.

RESULTS AND DISCUSSION

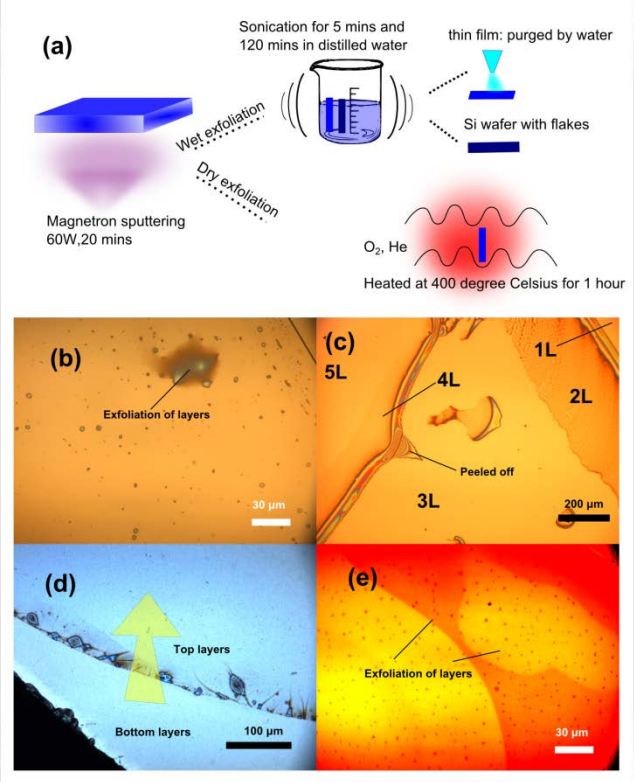

Figure 1 (a) The flow chart of the sample preparation. (b) The optical microscope images of the surface of W thin film sonicated for 5 mins, where the 2D layers start to be exfoliated. (c) The optical microscope images of the W thin film sonicated for 5 mins, where five 2D layers are exfoliated from the W thin film. (d) The optical microscope images of the W thin film sonicated for 120 min, where the 2D layer is exfoliated from the W thin film along the direction of yellow arrow. (e) The optical microscope images of the surface oxidized tungsten 2D layer from which the 2D layers are exfoliated.

Figure 1 (a) shows the flow chart of the sample preparation, where W thin film is deposited onto the Si wafer (coated with 5nm SiO_2) by RF sputtering. The power was kept at 60W for 20 mins. As-deposited W thin film contains a stack of 2D layers, where all the 2D layers are in a stack (referred as W thin film). In this paper, we applied two exfoliation methods: wet method and dry one. The wet method includes the sonication of tungsten thin film (light blue in Figure 1 (a)) and Si wafer (dark blue in Figure 1 (a)) in distilled water. The sonication durations are 5 mins and 120 mins, respectively. During the sonication, the flakes are dispersed into the distilled water, leaving a step-like profile on the surface of W thin film. Meanwhile, some flakes can reabsorb onto the surface of sample. In order to have clean surface, the tungsten thin film was purged with water to remove the attached flakes. The Si

wafer (dark blue one in Figure 1 (a)) was not purged in order to collect the flakes. After drying, the flakes were deposited onto the Si wafer. The tungsten samples in wet method are referred as “W sample”. The appearance of tungsten thin film after wet exfoliation has been shown in Figure S1. The thickness of the monolayer can be achieved by measuring the height of the step. The dry method includes the oxidization of the W thin film in a furnace with the flow of oxygen and helium. The temperature was kept at 400 degree Celsius for 1 hour. The growth of WO_3 layer exfoliates the adjacent monolayers. Although the W thin film is not fully oxidized, we still refer it as “WO_3 sample”.

Via the sonication in distilled water, the tungsten 2D layers in vicinity to the surface are firstly exfoliated into distilled water. As shown in Figure 1 (b), after 5 mins sonication, the exfoliation starts from one region with green and grey color. Afterwards, the 2D layers are dispersed into the distilled water.

After exfoliation, the steps of 2D layers appear on the surface. As shown in Figure 1 (c), five 2D layers were identified, where the 3rd layer is marked with the label “peeled off”. Generally, the W thin film has metallic and lustrous surface, which reflects the incident light [37]. However, the thin film can be transparent, if its thickness is reduced [38]. As shown in Figure 1 (d), the transparent topmost 2D monolayer was exfoliated in the direction of the yellow arrow.

The tungsten 2D layers were oxidized in an oven with the mixture of oxygen and helium flow (referred as WO_3 thin film). After oxidation, the thin film still keeps in a stack. As shown in Figure 1 (e), the contrast between dark and light part is possibly due to the exfoliation between the adjacent 2D monolayers with the help of oxide.

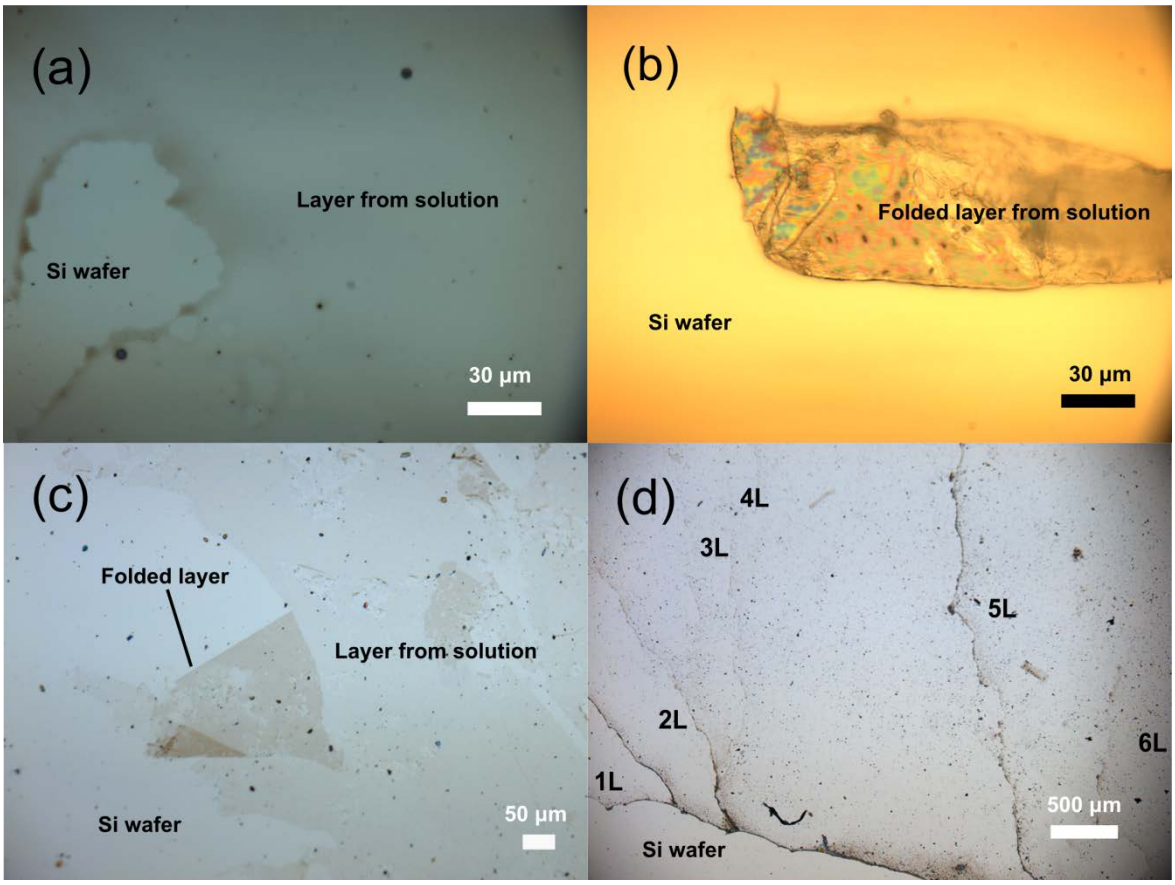

Figure 2 The free standing 2D layer transferred from the solution on the Si wafer. (a)The monolayer transferred from the solution after 5 mins sonication on the Si wafer. (b) The folded monolayer transferred from the solution after 10 mins sonication on the Si wafer. (c) The monolayer transferred from the solution after 120 mins sonication on the Si wafer. (d) The stack of monolayer (1L-6L) transferred from the solution after 120 mins sonication on the Si wafer.

From the wet exfoliation, we are able to obtain the very large size monolayers from the distilled water easily. During sonication, the tungsten 2D layers are exfoliated from the as deposited thin film. The free standing 2D layers can be deposited onto the silicon wafer. As discussed in Figure 1, the tungsten 2D monolayer is semitransparent. In Figure 2, the darker W monolayer is deposited on the Si wafer. In some cases, tungsten monolayer with large size can be folded after being transferred from the distilled water, as shown in Figure 2 (b). Figure 2 (c) shows a clear image of folded tungsten monolayer. However, the exfoliation of tungsten thin film in distilled water also results in a flake which consists of a stack of monolayers (1L to 6L), as shown in Figure 2 (d). The boundaries between tungsten monolayers are clearly visible.

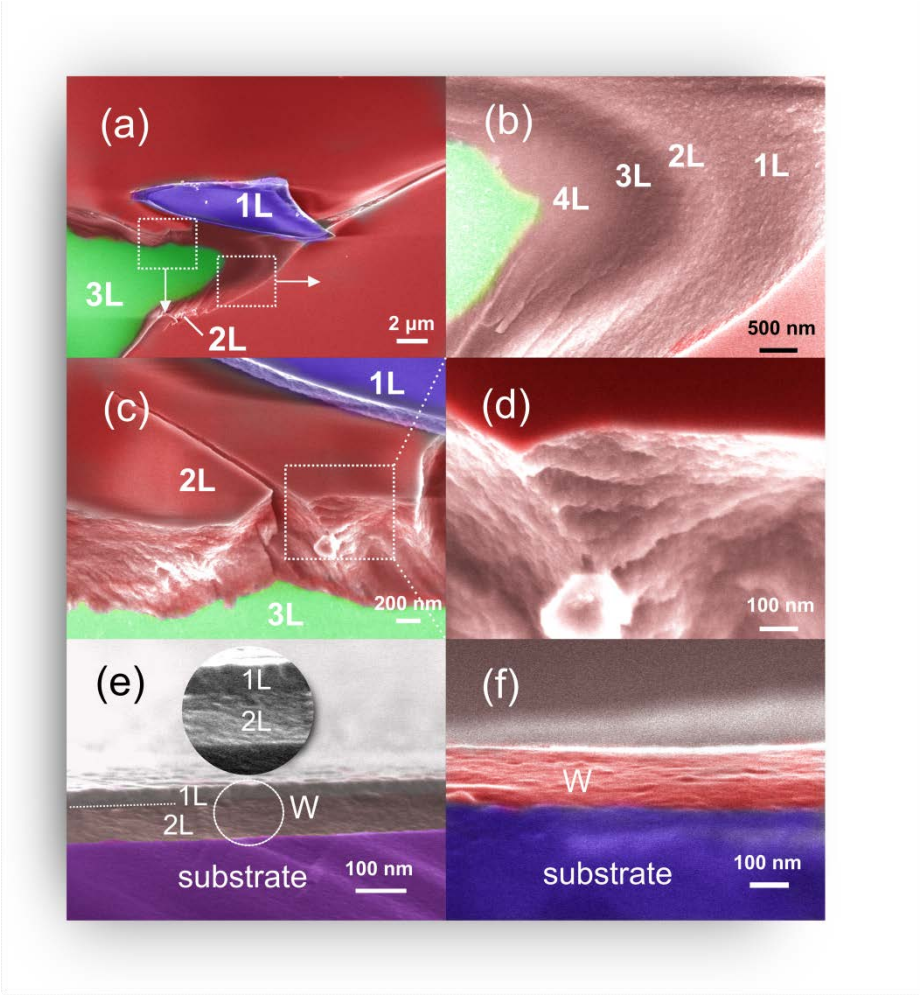

Figure 3 The morphologies of 2D monolayer (WO_3, W) in stack. (a) The low magnification SEM image of WO_3, where three layers (1L to 3L) are observed. (b) The SEM image in high magnification, which is enlarged from dashed square of Figure (a) marked with arrow. Four layers (1L to 4L) are identified. (c) The SEM (Scanning Electron Microscope) image in high magnification which is enlarged from dashed square of Figure (a) marked with arrow. 3 layers (1L to 3L) are observed. (d) Further enlarged SEM image from the dashed square of Figure (c). (e) The SEM images of the W thin film in cross sectional view, where 2 layers (1L to 2L) can be observed. The inserted image shows the enlarge part in the dash circle. (f) The SEM images of the W thin film in cross sectional view, where a stack of monolayers are identified.

The SEM images of sonicated W thin film are shown in the supplementary material (Figure S2 (a)-(c)). As the W thin film is oxidized in the mixture of oxygen and helium flow, the oxide coating is formed on 2D tungsten monolayers. Therefore, the 2D tungsten monolayers

are exfoliated with the help of surface oxide. The exfoliation leads to the formation of “bubbles” at the surface (Figure S2 (c)). In some cases, some of those “bubbles” can be collapsed after heating. The internal layered structure can be imaged at the edge of cracks. As shown in Figure 3 (a), 3 layers (1L-3L) are presented. However, the layers in Figure 3 (a) are not the thinnest one. From the cross sectional view in Figure 3(a), the 2L layer can be further divided into 4 layers in the dash square Figure 3 (b). Moreover, in the left dashed square in Figure 3 (a), the 2L layer consists of the thinnest monolayers. From the cross sectional view, the tungsten thin film also shows layered structure, as shown in Figure 3 (e) and (f). As shown in Figure 3 (e), two layers (1L to 2L) can be observed in the cross sectional view. The overall thickness of tungsten thin film is 100 nm. In Figure 3 (f), we can see a stack of tungsten monolayers within cross section of the tungsten thin film. The cross-sectional view of tungsten thin film was prepared by mechanical cleavage. More information can be found in Figure S2 (d)-(g).

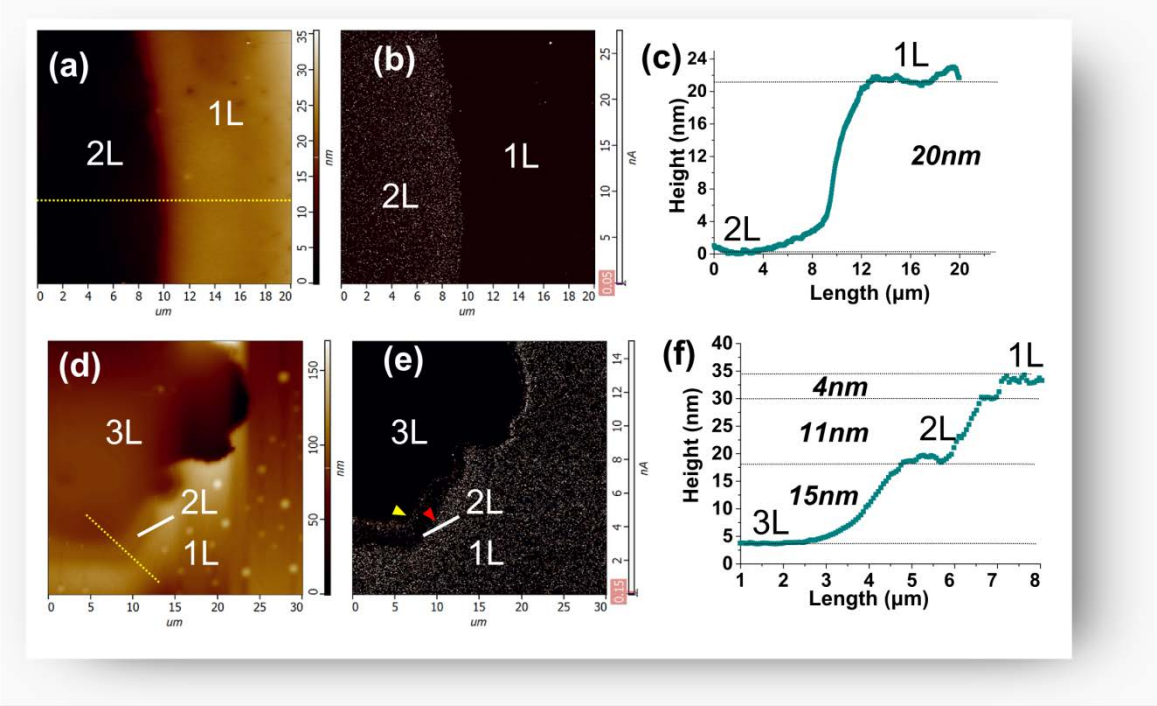

Figure 4 The conductive AFM images of samples. (a) The surface morphology of W thin film, sonicated for 5 mins, where 2 layers (1L, 2L) are marked. (b) The spread current map of W thin film in consistent with (a). (c) The profile of morphology, taken from the dash line in (a). (d) The surface morphology of WO_3 thin film, where 3 layers (1L to 3L) are marked. (e) The spread current map of WO_3 thin film is consistent with (d). (f) The profile of morphology, taken from the dash line in (d).

For the metallic 2D material, the most important properties are the thickness of 2D monolayer and the resistivity of 2D monolayer. However, the monolayer in Figure 2 is mechanically bonded to the substrate. The monolayer can be unstable during AFM scanning. In some cases, there might be air gap between the monolayer and substrate, which AFM measures larger thickness. Therefore, we mainly study the thickness of monolayer from the similar steps as shown in Figure 1 (c).

The tungsten 2D layer can be oxidized in the air [39],[40]. The tungsten oxide layer owns higher resistivity (630 Ω•cm), and behaves as insulating coating [41]. The conductive AFM captures the information of the surface morphology and current distribution simultaneously. During the scanning of conductive AFM, the tip is negatively biased at 0.12V, where the current flows from the tungsten thin film to the tip. Figure 4 (a)-(c) shows the surface morphology and spread current map in the W thin film sonicated for 5 mins. After sonication, some W layers have been exfoliated into the distilled water, leaving a step-like profile. The optical images of the areas measured by AFM are shown in Figure S3. In Figure 4 (a), a clear boundary separates the sample into two sections labeled with 1L and 2L. Due to the contact with oxygen in air, the surface is oxidized. From the spread current map in Figure 4 (b), the section of 2L layer (~8 MΩ) is more conductive in contrast with the section of 1L layer (~1.7 GΩ). The height of the step and hence the thickness of 1L monolayer, is 20 nm, as shown in Figure 4 (c). The W film sonicated for 120 mins is shown in Figure S4. As discussed above, the monolayers of tungsten thin film is bonded together after sonication. Therefore, the spread current contributes from the whole W thin film. After oxidation, each tungsten monolayer is covered with oxide. The monolayers are delaminated and insulated by the tungsten oxide. The spread current of individual tungsten monolayer covered by oxide can be measured.

The W film was oxidized in the mixture of oxygen and helium flow. As discussed in Figure 2, the adjacent monolayers are exfoliated and some defects, such as crack, may occur. Figure 4 (d)-(f) were taken from the edge of such cracks. From the Figure 4 (d), 3 layers were presented and with different thicknesses. The 1L layer in Figure 4(e) has a better conductivity (pointed by red arrow, ~24 MΩ) in comparison to 3L layer (approx. 80 MΩ). The less conductivity of 3L is possibly caused by the less conductive surface oxide. Moreover, the edge of 2L layer is conductive (pointed by yellow arrow, ~ 60 MΩ), which is referred as “conductive edge” in the following text.

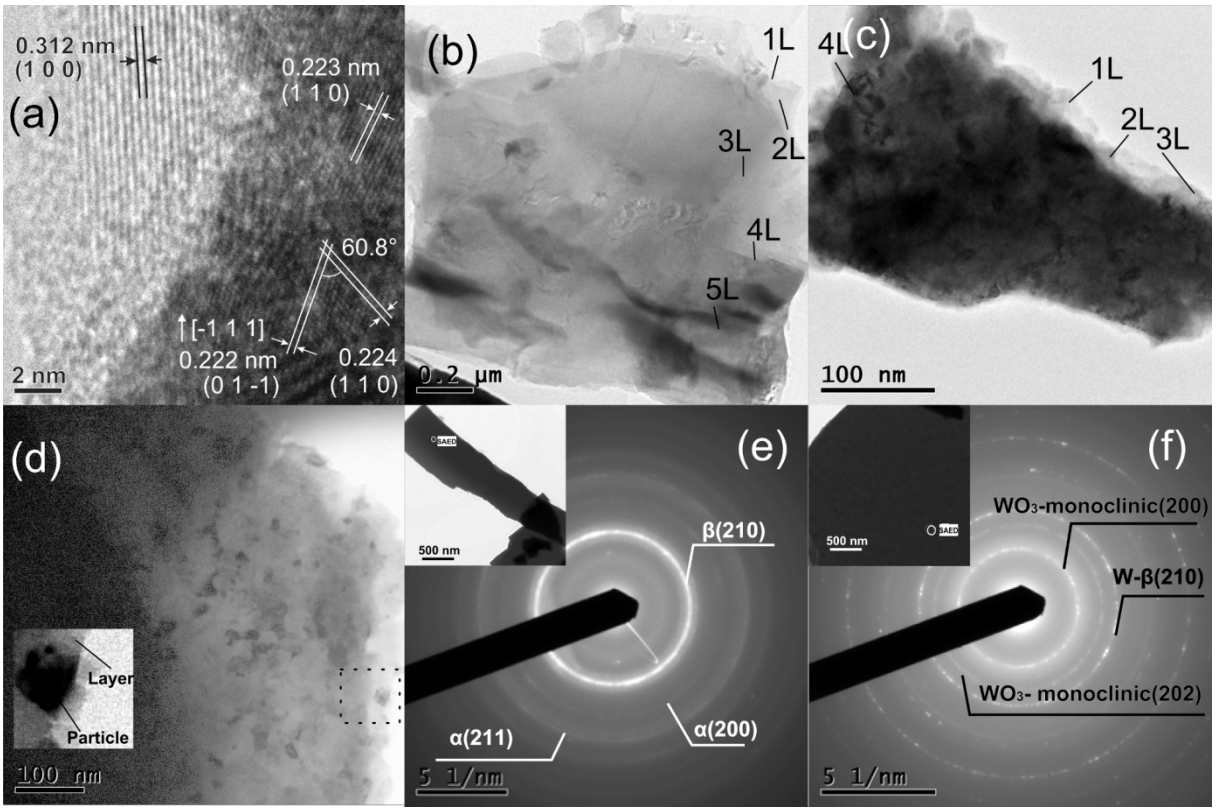

Figure 5 (a) HRTEM (High Resolution Transmission Electron Microscope) image of W layers at high magnification (b) HRTEM image of W layers at low magnification. The sequence of layers is marked from 1L to 5L. (c) The HRTEM image of WO_3 layers. The sequence of layers is marked from 1L to 4L. (d) The HRTEM image of WO_3 layers. The black particle in the dashed square is enlarged in the inlet image (left). (e) SAED (Selected area diffraction) pattern of W. The inlet image shows the HRTEM images from where the place of SAED was taken. (f) SAED (Selected area diffraction) pattern of WO_3 thin film.

The as-deposited W and oxidized WO_3 sample were scratched from substrate and transferred to carbon thin film for HRTEM imaging. The thinnest part of scratched sample lies at the edge, which consists of serveral monolayers. Therefore, The lattice fringes of tungsten 2D layer can be seen at the very edge of sample in Figure 5 (a). The W lattice spacings of (110) and (011) are 0.224 nm and 0.222 nm, respectively. The dihedral angle is 60.8 degree. The

SAED (Selected area diffraction) pattern in Figure S6 further proves presence of α-phase tungsten in Figure 5 (a).

The five layers of the W sample are clearly visible in Figure 5 (b). And the thinnest part is in the edge of sample with the monolayer 1L-2L. It was also possible to observe the delamination between monolayer 5L and 4L. Figure 5 (c) shows the WO_3 sample, where four 2D monolayers are marked at the very edge of sample. In comprasion with Figure 5 (b), the layers in Figure 5 (c) are much darker and opague in the middle of the sample, which is possibly caused by the presence of tungsten oxide. Figure 5 (d) shows the edge of WO_3 sample. The particle in the dash square in Figure 5 (d) is possibly WO_3 which seperates the adjacent tungsen 2D monolayer.

The SAED patterns of W and WO_3 are shown in Figure 5 (e)-(f). The inserted HRTEM image shows the place from where SAED was taken. The center part of the sample has larger thickness in comparation with the very edge of the sample. We can find the coexistence of tungsten α and β phases, other than oxide. As discussed in Figure 4 (b), the surface of tungsten is naturelly oxidized in the air. Therefore, the oxide coating is either too thin or in amorphous state. The WO_3 is in monoclinic structure with presence of the β phase tungsten after oxidation, as shown in Figure 5(f). The result proves the tungsten film is not fully oxidized in the furnace.

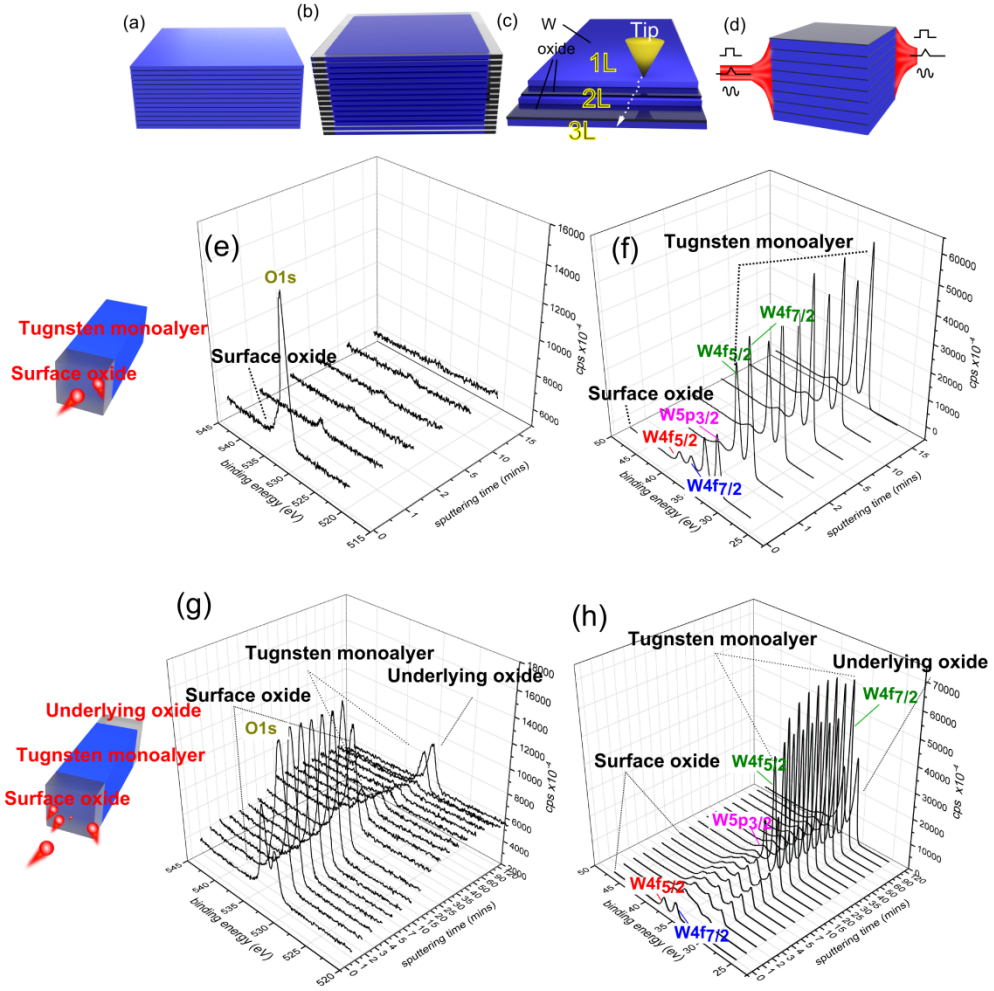

Figure 6 (a) The schematic model of as-deposited tungsten film in 2D layers stack. The blue monolayers are tungsten. (b) The schematic model of WO_3 layers stack. The blue tungsten monolayer is coated with the transparent oxide. (c) The model explains the "conductive edge" in Figure 4 (e). The yellow cone represents AFM tip. The layer is marked according to Figure 4 (e). (d) The application of 2D metal stack. The blue monolayers are separated by the grey oxide layers. Each monolayer is equivalent to one channel for signal transport. (e) O1s XPS spectra of the tungsten thin film, changing with the sputtering time in XPS instrument. The inlet image shows the scheme of tungsten monolayer with surface oxide. (f) W4f XPS spectra of tungsten monolayer in dependence on the sputtering time. (g) O1s XPS spectra of the tungsten monolayer after oxidation (in a furnace with the mixture of oxygen and helium flow) in dependence on the sputtering time. The inlet image shows the scheme of tungsten oxide thin film. (h) W4f XPS spectra of the tungsten monolayer after oxidation (in a furnace with the

mixture of oxygen and helium flow) in dependence on the sputtering time. The inlet image shows the scheme of tungsten oxide thin film.

We demonstrated that the sputtered W thin film is layered, as shown schematically in Figure 6 (a). During sputtering, the heat is transferred continuously from the plasma and the vapor to the silicon substrate. Therefore, the silicon substrate keeps expanding. Therefore, the continuous growth of thin film is interrupted by the thermal expansion time to time. And the layers are formed during sputtering. The detail is discussed in Figure S9. Before oxidation, all the tungsten monolayers are bonded in a stack, where the current can flow vertically and horizontally. During oxidation, the W monolayers are coated with oxide, as shown schematically in Figure 6 (b). In this case, the tungsten monolayers are exfoliated. And the insulating oxide blocks the current flowing between different tungsten monolayers. Therefore, the current is able to flow along each tungsten monolayer. Figure 6 (c) depicts the model to explain experimental observation described in Figure 4 (d)-(f), where the oxide 2D layer is relatively insulating and the tungsten 2D layer is conductive. During the breakdown of the "bubble" shown in Figure S2 (c), some oxide coating are peeled off from the tungsten monolayer. Therefore, it can explain the higher conductivity in 1L (Figure 4(e)) which should be coated with oxide. Moreover, the monolayer 2L (Figure 4(e)) has a conductive edge, which is possibly induced by the mismatch of oxide coating and tungsten monolayer.

The layered tungsten or the other metals can be, in our opinion, used for transport of electric signals, as shown in Figure 6 (d). Each 2D monolayer is disconnected and insulated by the oxide layer. Therefore, one tungsten wire in circuit contains multiple channels. The signal is able to be transported along the metallic monolayers. The quality of self-assembled 2D layers W and WO_3 is far to ideal and still needs further development.

As discussed above, the model of the monolayers structure has been presented in Figure 6 (b) and (d), where each tungsten layer is coated with the oxide after oxidation. XPS is widely used to determine the composition of metal and oxides [42]. Figure 6 (e) shows a change of the XPS spectra (tungsten monolayer) with the sputtering time. The area of O1s signal at 523 eV decreases dramatically after 1 minutes sputtering. As discussed in Figure 4(b), the tungsten thin film is oxidized in the air. The most of surface tungsten oxide is sputtered away in XPS instrument within 1 minute. XPS spectra of W4f peaks also prove the same conclusion, as shown in Figure 6 (f). The strong doublet peaks ($W4f_{7/2}$ and $W4f_{5/2}$) at 31.3 eV and 33.4 eV can be attributed to the metallic W, of which XPS peak area increases after 1 minute

sputtering. The doublet peaks of W monolayer at 36.7 eV and 34 eV are assigned to the tungsten oxide (WO_3), which disappears after 1 minute sputtering. By comparison with the spectra in Figure 6 (e), the surface tungsten oxide layer shown in in Figure 6 (g) is much thicker due to sample oxidation (in a furnace with the mixture of oxygen and helium flow). The area of peaks in O1s signal decreases after 35 minutes sputtering and starts to increase after 90 minutes sputtering. The variation trend of tungsten oxide presence fits with the inserted 3D model shown in Figure 6 (g). The XPS spectra of W4f metal and oxide are presented in Figure 6 (h). Before sputtering, the oxide W4f doublet pairs are clearly visible. With the increase of sputtering time, the more WO_3 is removed from the surface. The area of metallic tungsten W4f doublet peaks increase dramatically from 20th minutes of sputtering. Based on that, we believe the surface oxide has been removed and the underlying tungsten monolayer has been reached. With the further sputtering the area of metallic W4f doublet peaks drops. As the result of that, the sputtering reached the boundary between tungsten monolayer and the underlying oxide layer. The result supports the model presented in Figure 6(b).

CONCLUSIONS

In this paper, we report the study of 2D tungsten material. The tungsten thin film was prepared by magnetron sputtering. The structure of as sputtered tungsten thin film is layered. The ultra large monolayer can be obtained from the layered tungsten thin film via wet exfoliation by sonication in distilled water.

Besides the wet exfoliation method, the W is oxidized in an oven with the mixture of oxygen and helium flow, which is referred to dry exfoliation method. In such process, the growing WO_3 electrically isolates each tungsten 2D monolayer. However, the tungsten 2D monolayers within stack remain electrically conductive.

The morphology of tungsten thin film was studied via optical microscopy, SEM, AFM and HRTEM. The side view and top view of the tungsten thin film show a layered structure with monolayers in different thickness. Based on the facts above, we put forward the structural model of layered tungsten thin film. The XPS study proves the model in the view of chemical composition (e.g. existence of alternating monolayers $WO_3/W/WO_3$ after dry exfoliation). However, there is still large space to develop this method. For instance, the origin of layer

forming is still unclear. Probably, the expansion or contraction of the substrate can be one of the important factors. The expansion of the substrate depends on the heat generated and transferred from the sputtering process. Nevertheless, preparation of 2D metallic material by magnetron sputtering is still a simple and effective method.

ACKNOWLEDGMENTS

The authors thank for financial support from the grant of the Ministry of Education, Youth and Sports of Czech Republic (grant LM2015082), the European Regional Development Fund-Project "Modernization and upgrade of the CEMNAT" (No.CZ.02.1.01/0.0/0.0/16_013/0001829), and the project of Czech Grant Agency (GA CR) 19-20792S.

[1] K.S. Novoselov, A.K. Geim, S. V. Morozov, D. Jiang, Y. Zhang, S. V. Dubonos, I. V. Grigorieva, A.A. Firsov, Electric field in atomically thin carbon films, Science (80-.). 306 (2004) 666–669. https://doi.org/10.1126/science.1102896.

[2] H. Zhang, Ultrathin Two-Dimensional Nanomaterials, ACS Nano. 9 (2015) 9451–9469. https://doi.org/10.1021/acsnano.5b05040.

[3] U. Younis, I. Muhammad, Y. Kawazoe, Q. Sun, Design of tetracene-based metallic 2D carbon materials for Na- and K-Ion batteries, Appl. Surf. Sci. 521 (2020) 146456. https://doi.org/10.1016/j.apsusc.2020.146456.

[4] Z. Chen, Y. Yu, X. She, K. Xia, Z. Mo, H. Chen, Y. Song, J. Huang, H. Li, H. Xu, Constructing Schottky junction between 2D semiconductor and metallic nickel phosphide for highly efficient catalytic hydrogen evolution, Appl. Surf. Sci. (2019). https://doi.org/10.1016/j.apsusc.2019.07.270.

[5] D.A. Olyanich, V. V. Mararov, T. V. Utas, L. V. Bondarenko, A.Y. Tupchaya, A. V. Matetskiy, N. V. Denisov, A.N. Mihalyuk, S. V. Eremeev, D. V. Gruznev, A. V. Zotov, A.A. Saranin, C60 capping of metallic 2D Tl-Au compound with preservation of its basic properties at the buried interface, Appl. Surf. Sci. (2020). https://doi.org/10.1016/j.apsusc.2019.144253.

[6] Y. Ma, B. Li, S. Yang, Ultrathin two-dimensional metallic nanomaterials, Mater. Chem. Front. 2 (2018) 456–457. https://doi.org/10.1039/c7qm00548b.

[7] X. Huang, Z. Zeng, H. Zhang, Metal dichalcogenide nanosheets: Preparation, properties and applications, Chem. Soc. Rev. 42 (2013) 1934–1946. https://doi.org/10.1039/c2cs35387c.

[8] R. Ma, T. Sasaki, Two-dimensional oxide and hydroxide nanosheets: Controllable high-quality exfoliation, molecular assembly, and exploration of functionality, Acc. Chem. Res. 48 (2015) 136–143. https://doi.org/10.1021/ar500311w.

[9] J.W. Colson, W.R. Dichtel, Rationally synthesized two-dimensional polymers, Nat. Chem. 5 (2013) 453–465. https://doi.org/10.1038/nchem.1628.

[10] J. Shamsi, Z. Dang, P. Bianchini, C. Canale, F. Di Stasio, R. Brescia, M. Prato, L. Manna, Colloidal Synthesis of Quantum Confined Single Crystal CsPbBr3 Nanosheets with Lateral Size Control up to the Micrometer Range, J. Am. Chem. Soc. 138 (2016) 7240–7243. https://doi.org/10.1021/jacs.6b03166.

[11] Y. Li, W. Wang, K. Xia, W. Zhang, Y. Jiang, Y. Zeng, H. Zhang, C. Jin, Z. Zhang, D. Yang, Ultrathin Two-Dimensional Pd-Based Nanorings as Catalysts for Hydrogenation with High Activity and Stability, Small. 11 (2015) 4745–4752. https://doi.org/10.1002/smll.201500769.

[12] X. Huang, Y. Li, Y. Chen, H. Zhou, X. Duan, Y. Huang, Plasmonic and catalytic AuPd nanowheels for the efficient conversion of light into chemical energy, Angew. Chemie - Int. Ed. 52 (2013) 6063–6067. https://doi.org/10.1002/anie.201301096.

[13] Z. Fan, M. Bosman, X. Huang, D. Huang, Y. Yu, K.P. Ong, Y.A. Akimov, L. Wu, B. Li, J. Wu, Y. Huang, Q. Liu, C. Eng Png, C. Lip Gan, P. Yang, H. Zhang, Stabilization of 4H hexagonal phase in gold nanoribbons, Nat. Commun. 6 (2015). https://doi.org/10.1038/ncomms8684.

[14] Y. Chen, C. Somsen, S. Milenkovic, A.W. Hassel, Fabrication of single crystalline gold nanobelts, J. Mater. Chem. 19 (2009) 924–927. https://doi.org/10.1039/b816897k.

[15] M. Maillard, S. Giorgio, M.P. Pileni, Silver nanodisks, Adv. Mater. 14 (2002) 1084–1086. https://doi.org/10.1002/1521-4095(20020805)14:15<1084::AID-ADMA1084>3.0.CO;2-L.

[16] Y. Xiong, J.M. McLellan, J. Chen, Y. Yin, Z.Y. Li, Y. Xia, Kinetically controlled synthesis of triangular and hexagonal nanoplates of palladium and their SPR/SERS properties, J. Am. Chem. Soc. 127 (2005) 17118–17127. https://doi.org/10.1021/ja056498s.

[17] Y. Chen, Z. Fan, Z. Zhang, W. Niu, C. Li, N. Yang, B. Chen, H. Zhang, Two-Dimensional Metal Nanomaterials: Synthesis, Properties, and Applications, Chem. Rev. 118 (2018) 6409–6455. https://doi.org/10.1021/acs.chemrev.7b00727.

[18] H.L. Qin, D. Wang, Z.L. Huang, D.M. Wu, Z.C. Zeng, B. Ren, K. Xu, J. Jin, Thickness-controlled synthesis of ultrathin au sheets and surface plasmonic property, J. Am. Chem. Soc. 135 (2013) 12544–12547. https://doi.org/10.1021/ja406107u.

[19] X. Huang, S. Li, Y. Huang, S. Wu, X. Zhou, S. Li, C.L. Gan, F. Boey, C.A. Mirkin, H. Zhang, Synthesis of hexagonal close-packed gold nanostructures, Nat. Commun. 2 (2011). https://doi.org/10.1038/ncomms1291.

[20] H. Liu, H. Tang, M. Fang, W. Si, Q. Zhang, Z. Huang, L. Gu, W. Pan, J. Yao, C. Nan, H. Wu, 2D Metals by Repeated Size Reduction, Adv. Mater. (2016) 8170–8176. https://doi.org/10.1002/adma.201601180.

[21] J. Gu, B. Li, Z. Du, C. Zhang, D. Zhang, S. Yang, Multi-Atomic Layers of Metallic Aluminum for Ultralong Life Lithium Storage with High Volumetric Capacity, Adv. Funct. Mater. 27 (2017). https://doi.org/10.1002/adfm.201700840.

[22] N. Hussain, T. Liang, Q. Zhang, T. Anwar, Y. Huang, J. Lang, K. Huang, H. Wu, Ultrathin Bi Nanosheets with Superior Photoluminescence, Small. 13 (2017). https://doi.org/10.1002/smll.201701349.

[23] J. Zhuang, N. Gao, Z. Li, X. Xu, J. Wang, J. Zhao, S.X. Dou, Y. Du, Cooperative Electron-Phonon Coupling and Buckled Structure in Germanene on Au(111), ACS Nano. 11 (2017) 3553–3559. https://doi.org/10.1021/acsnano.7b00687.

[24] P. Ares, F. Aguilar-Galindo, D. Rodríguez-San-Miguel, D.A. Aldave, S. Díaz-Tendero, M. Alcamí, F. Martín, J. Gómez-Herrero, F. Zamora, Mechanical Isolation of Highly Stable Antimonene under Ambient Conditions, Adv. Mater. (2016) 6332–6336. https://doi.org/10.1002/adma.201602128.

[25] J. Zhuang, X. Xu, G. Peleckis, W. Hao, S.X. Dou, Y. Du, Silicene: A Promising Anode for Lithium-Ion Batteries, Adv. Mater. 29 (2017). https://doi.org/10.1002/adma.201606716.

[26] X.-F. Zhai, H. Shan, L.-F. Zhang, Z.-P. Hu, Y.-H. Mao, A.-D. Zhao, B. Wang, H.-L. Wang, Epitaxial growth of highly strained antimonene on Ag(111), Front. Phys. 13 (2018) 138106. https://doi.org/10.1007/s11467-018-0757-3.

[27] S.R. Tavares, P.I.R. Moraes, R.B. Capaz, A.A. Leitão, Novel 2D materials from exfoliation of layered hydroxide salts: A theoretical study, Appl. Surf. Sci. (2019). https://doi.org/10.1016/j.apsusc.2019.03.144.

[28] J. Zhao, Q. Deng, A. Bachmatiuk, G. Sandeep, A. Popov, J. Eckert, M.H. Rümmeli, Free-standing single-atom-thick iron membranes suspended in graphene pores, Science (80-.). 343 (2014) 1228–1232. https://doi.org/10.1126/science.1245273.

[29] L.M. Liz-Marzán, M. Grzelczak, Growing anisotropic crystals at the nanoscale, Science (80-.). 356 (2017) 1120–1121. https://doi.org/10.1126/science.aam8774.

[30] J. Niu, D. Wang, H. Qin, X. Xiong, P. Tan, Y. Li, R. Liu, X. Lu, J. Wu, T. Zhang, W. Ni, J. Jin, Novel polymer-free iridescent lamellar hydrogel for two-dimensional confined growth of ultrathin gold membranes, Nat. Commun. 5 (2014). https://doi.org/10.1038/ncomms4313.

[31] Z. Fan, X. Huang, C. Tan, H. Zhang, Thin metal nanostructures: Synthesis, properties and applications, Chem. Sci. 6 (2015) 95–111. https://doi.org/10.1039/c4sc02571g.

[32] Y. Yang, X.L. Zhong, Q. Zhang, L.G. Blackstad, Z.W. Fu, Z.Y. Li, D. Qin, The role of etching in the formation of ag nanoplates with straight, curved and wavy edges and comparison of their SERS properties, Small. 10 (2014) 1430–1437. https://doi.org/10.1002/smll.201302877.

[33] L.R. Hirsch, R.J. Stafford, J.A. Bankson, S.R. Sershen, B. Rivera, R.E. Price, J.D. Hazle, N.J. Halas, J.L. West, Nanoshell-mediated near-infrared thermal therapy of tumors under magnetic resonance guidance, Proc. Natl. Acad. Sci. 100 (2003) 13549–13554. https://doi.org/10.1073/pnas.2232479100.

[34] A.P. Kulkarni, K.M. Noone, K. Munechika, S.R. Guyer, D.S. Ginger, Plasmon-enhanced charge carrier generation in organic photovoltaic films using silver nanoprisms, Nano Lett. 10 (2010) 1501–1505. https://doi.org/10.1021/nl100615e.

[35] B. Zhang, T. Mikysek, V. Cicmancova, S. Slang, R. Svoboda, P. Kutalek, T. Wagner, 2D GeSe2 amorphous monolayer, in: Pure Appl. Chem., 2019. https://doi.org/10.1515/pac-2019-0501.

[36] B. Zhang, V. Cicmancova, J. Kupcik, S. Slang, J. Rodriguez Pereira, R. Svoboda, P. Kutalek, T. Wagner, A layered Ge 2 Sb 2 Te 5 phase change material, Nanoscale. 12 (2020) 3351–3358. https://doi.org/10.1039/C9NR08745A.

[37] J. Lekner, Theory of Reflection of Electromagnetic and Particle Waves, 1987. https://doi.org/10.1007/978-94-015-7748-9.

[38] M. Avrekh, B.M. Thibadeau, O.R. Monteiro, I.G. Brown, Transparent, conducting, metallic thin films, Rev. Sci. Instrum. 70 (1999) 4328–4330. https://doi.org/10.1063/1.1150075.

[39] Y. Kamiura, K. Umezawa, Y. Teraoka, A. Yoshigoe, Characterization of polycrystalline tungsten surfaces irradiated with nitrogen ions by X-ray photoelectron spectroscopy, Nippon Kinzoku Gakkaishi/Journal Japan Inst. Met. 81 (2017) 510–515. https://doi.org/10.2320/jinstmet.J2017009.

[40] W. Lisowski, A.H.J. van den Berg, G.A.M. Kip, L.J. Hanekamp, Characterization of tungsten tips for STM by SEM/AES/XPS, Fresenius. J. Anal. Chem. 341 (1991) 196–199. https://doi.org/10.1007/BF00321548.

[41] K. Aguir, C. Lemire, D.B.B. Lollman, Electrical properties of reactively sputtered WO3 thin films as ozone gas sensor, Sensors Actuators, B Chem. 84 (2002) 1–5. https://doi.org/10.1016/S0925-4005(02)00003-5.

[42] M.C. Biesinger, B.P. Payne, A.P. Grosvenor, L.W.M. Lau, A.R. Gerson, R.S.C. Smart, Resolving surface chemical states in XPS analysis of first row transition metals, oxides and hydroxides: Cr, Mn, Fe, Co and Ni, Appl. Surf. Sci. (2011). https://doi.org/10.1016/j.apsusc.2010.10.051.